3D Reconstruction of Volume Defects from few X-ray Images

C. Lehr, C.-E. Liedtke

Institut für Theoretische Nachrichtentechnik und Informationsverarbeitung,
Division: Automatic Image Interpretation, Prof. Dr.-Ing. C.-E. Liedtke,
Universität Hannover, Appelstr. 9A, 30167 Hannover, Germany
Phone: +49-511-7625328, Fax: +49-511-7625333, Email: lehr@tnt.uni-hannover.de

Abstract. In nondestructive testing for quality control of industrial objects the standard X-ray analysis produces a 2D projection of the 3D objects. Defects can be detected but cannot be localized in 3D position, size and shape. Tomographic testing equipment turns frequently out to be too costly and time consuming for many applications. Here a new approach for 3D reconstruction is suggested using standard X-ray equipment without costly positioning equipment. The new approach requires only a small number of X-ray views from different directions in order to reduce the image acquisition time.
The geometric and photometric imaging properties of the system are calibrated using different calibration patterns. The parameters of a CAHV camera model are obtained for each view permitting the exact registration of the acquired images. The efficiency of the 3D reconstruction algorithm has been increased by limiting the reconstruction to regions of interest around the defects. This requires an automated segmentation. The 3D reconstruction of the defects is performed with an iterative procedure. Regularization of the reconstruction problem is achieved on the basis of the maximum entropy principle. The reliability and robustness of the method has been tested on simulated and real data.

Keywords: X-ray, tomography, calibration

1 Motivation

Non destructive testing constitutes a major part of quality control in industrial production. The standard X-ray analysis produces a 2D projection of the 3D objects. Defects can be detected but cannot be localized in 3D position, size, and shape. For this purpose tomographic testing equipment has to be used which is described at several places in the literature [1],[2]. The use of tomographic testing methods within industrial quality control is limited by several facts. Traditional tomographic systems are too complex and expensive for several applications. They require usually sophisticated detectors and very accurate and expensive mechanical devices for positioning. The inspection time which is caused by the analysis of a large number of views taken from around the object

is often considered to be too long [3],[4]. Frequently it is the aspect ratio of the test objects which prevents the radiographic analysis from all sides for the volume reconstruction as in the case of platelike objects. For these reasons there exists a demand for tomographic systems, which operate on the basis of simple radiographs and which permit the volume reconstruction from a small number of views. The first aspect would tend to reduce the costs, the second to reduce the time for the analysis. In connection with the reduction of the number of views as compared to standard tomographic equipment additional problems become apparent. The reconstruction problem becomes strongly underdetermined and may produce inconsistent results due to calibration errors, noise and other effects and the conventional tomographic algorithms like filtered backprojection, transformation methods, etc are not suitable anymore. Additional information like prior information about the geometry or material properties of the object under investigation is needed in order to arrive at a unique solution.

A special application is the reconstruction of casting defects, i.e. the reconstruction of an inclusion like gas within an otherwise homogeneous object. In this case the image reconstruction problem can be reduced to the estimation of binary object properties, i.e. object material vs. inclusion. Different approaches have been suggested in the literature [5],[6] where some of them require the use of parametrized functions in order to describe the objects under investigation. Because of the large variety of possible casting defects these model based approaches do not seem to be suitable or seem at least to limit the scale of possible applications. Other approaches are based on modelling the image as a binary Markov random field [7],[3]. The reconstruction is achieved by minimizing an error function dependent on the measured projections and on a a-priori choice of image modelling assumptions. The main difficulty of this type of approach is to achieve a reasonable fast and reliable minimization considering the very large number of unknown voxels.

In this paper a two-stage procedure for the 3D reconstruction of volume defects from a few radiographs is presented, which exploits the prior knowledge of the material parameters. No a-priori assumptions about the shape of the object under investigation have to be made. An overview about the processing steps is depicted in Fig. 1. After a calibration of the projective properties of the imaging device and a registration of the different views the complexity of the reconstruction problem is reduced in a first step by limiting the reconstruction to regions of interest around the defects. The defect areas are segmented and the spatial extent of the defects in beam direction is estimated from the measured data using calibration curves. In a second step the defects are reconstructed with an iterative procedure. Regularization of the reconstruction problem is achieved on the basis of the maximum entropy principle in connection with an iterative procedure for the binarization of the reconstruction results. In Chapter 2 the camera model and the calibration procedure is explained. Chapter 3 describes the segmentation process and Chapter 4 the procedure for the 3D reconstruction. Finally in Chapter 5 results are presented based on simulated and real data.

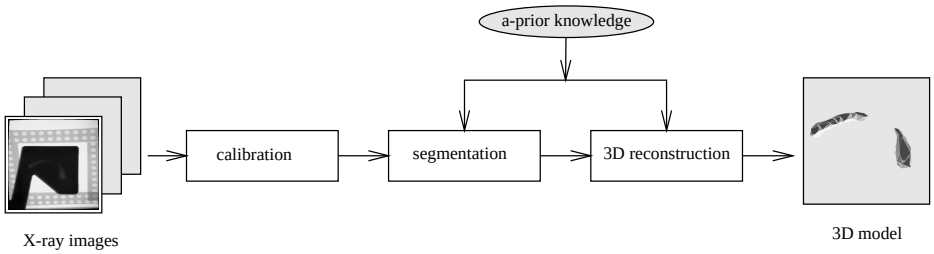

Fig. 1. System overview

2 Camera Parameters

The components of the X-ray system are depicted in Fig. 2. A microfocus X-ray tube serves as X-ray source. For imaging an image intensifier and a CCD-camera are used. The focus of the radiation-source is in the magnitude of μm and serves effectively as point source. The rays which traverse the test object are attenuated according to its geometric and material properties. The mapping process of the rays can be described by perspective projection. The imaging system itself exhibits a number of (primary radial) geometric distortions. This is partly due to the spheric shaped screen of the image intensifier, partly caused by magnetic fields which influence the electronic beam and other reasons. The radial distortions of the optical system of the CCD-camera appear to be much smaller and can be neglected.

The imaging properties of the system are mathematically described by the camera model. The parameters of the camera model are estimated in an calibration procedure using a calibration pattern. Since for tomographic reconstructions several camera views of the same object are required, the images have to be registered. For this purpose test object and calibration pattern need to remain in a fixed position relative to each other during the image acquisition step. The calibration procedure is applied to each viewing position in order to obtain precise position parameters for each individual view. The nonlinear geometric distortions are considered in a second step following the perspective projection.

For modelling the perspective projection the CAHV camera model from Yakimovski and Cunningham [8] has been employed using the following nomenclature:

$\boldsymbol{C}$: position of the radiation source in space
$\boldsymbol{H_0}$: unit vector pointing in the horizontal direction of the imaging target
$\boldsymbol{V_0}$: unit vector pointing in the vertical direction of the imaging target
$\boldsymbol{A}$: unit vector describing the optical axis
h_x and h_y: image point where the optical axis traverses the imaging target
s_x, s_y: pixel size
f: distance of radiation source from imaging plane.

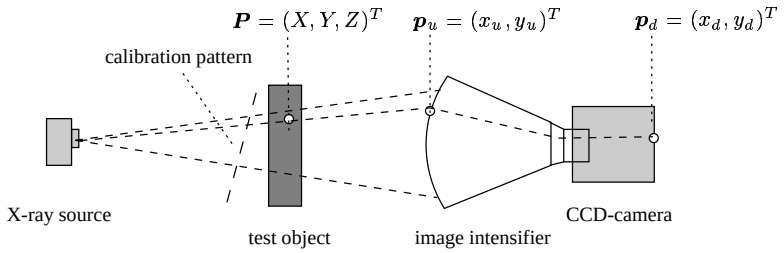

Fig. 2. Components of the X-ray system

Following the principles of geometric projection a point $\boldsymbol{P}$ in space is projected onto a point $\boldsymbol{p_u}$ in the image plane disregarding geometrical distortions following Eq. 1.

$$\boldsymbol{p_u} = \begin{pmatrix} x_u \\ y_u \end{pmatrix} = \frac{1}{\boldsymbol{A}^T \cdot (\boldsymbol{P} - \boldsymbol{C})} \cdot \begin{pmatrix} (f/s_x \cdot \boldsymbol{H_0} + h_x \cdot \boldsymbol{A})^T \cdot (\boldsymbol{P} - \boldsymbol{C}) \\ (f/s_y \cdot \boldsymbol{V_0} + h_y \cdot \boldsymbol{A})^T \cdot (\boldsymbol{P} - \boldsymbol{C}) \end{pmatrix} \tag{1}$$

The line of projection from the radiation source to an image point $\boldsymbol{p_u}$ is calculated as

$$\boldsymbol{S}(\boldsymbol{p_u}) = \boldsymbol{C} + s \cdot \boldsymbol{S_0}(\boldsymbol{p_u}) \tag{2}$$

where $\boldsymbol{S}_0(\boldsymbol{p_u})$ represents the line of sight. The intensity of the beam is attenuated according to the geometric extensions along the line of sight depending on the material properties and the particular spectrum of the radiation source as described in Eq. 3.

$$i(\boldsymbol{p_u}) = \int_{W_{min}}^{W_{max}} \left(i_0(\boldsymbol{p_u}) \cdot \exp\left(- \int_0^{s_{BV}} \mu\left(\boldsymbol{S}(\boldsymbol{p_u})\right) \, ds \right) \right) dW \tag{3}$$

In Eq. 3 $i_0(\boldsymbol{p_u})$ refers to the un-attenuated intensity in the image point $\boldsymbol{p_u}$ and W to a particular wavelength of the radiation source.

Geometrical distortions are corrected according to Eq. 4 using two-dimensional polynomial functions. The parameters of these two-dimensional functions have been estimated during a separate calibration process employing a planar calibration pattern with equidistant calibration marks. The coefficients of the polynomials have been obtained during an optimization procedure, where the mean squared distance between the estimated positions of the calibration marks and their prior known correct positions has been minimized [9]. From the calibration the pixel size s_x and s_y are obtained as well.

The calibration remains valid as long as the geometric relation between radiation source and the imaging device does not change.

$$\boldsymbol{p_d} = \begin{pmatrix} x_d \\ y_d \end{pmatrix} = \begin{pmatrix} f_1(x_u, y_u) \\ f_2(x_u, y_u) \end{pmatrix} \tag{4}$$

$$f_1(), f_2() : polynomial functions$$

The estimation of the parameters of the projection model is done for each individual position in the sequence of camera views which are acquired for one tomographic reconstruction. The setup is indicated in Fig. 3. The test object under investigation is recorded together with a calibration pattern. The calibration pattern consists of a planar plate with circular calibration marks arranged on its periphery. The presence of the calibration pattern does not affect the analysis of the investigated object. It reduces only the image area which can be utilized. The calibration procedure does not require the use of all calibration marks but only those which are detected with a high degree of reliability.

The parameter estimation uses a modified version of the method described by Tsai [10] for the calibration of CCD-cameras. It works iteratively starting with a reduced set of parameters and increases the number of parameters step by step. Since the camera parameters influence each other small errors in the localization of the calibration marks may result in significant errors of the derived camera parameters. The reliability can be improved by increasing the number of measurements. This can be achieved by using the measurements from several views for the estimation of those parameters which remain constant in all views, the so called inner camera parameters f, h_x and h_y.

3 Image Segmentation

The efficiency of the tomographic reconstruction could be increased considerably by reducing the reconstruction problem to the area which contains the defects. This requires an automated segmentation of the images which will be used for the reconstruction. The steps of the image segmentation procedure are shown in Fig. 4.

In a first step the measured intensity values $i(\boldsymbol{p_u})$ are converted into estimates for the material thickness $g_b(\boldsymbol{p_u})$ using a calibration function G.

$$g_b(\boldsymbol{p_u}) = G\left(i(\boldsymbol{p_u})\right) \tag{5}$$

This is referred to in Fig. 4 by the term "linearization". G depends on the intensity and the spectrum of the radiation source and the material of the object under investigation. In order to consider different radiation effects like backscattering the calibration function is obtained from experiments using calibration objects of different thickness.

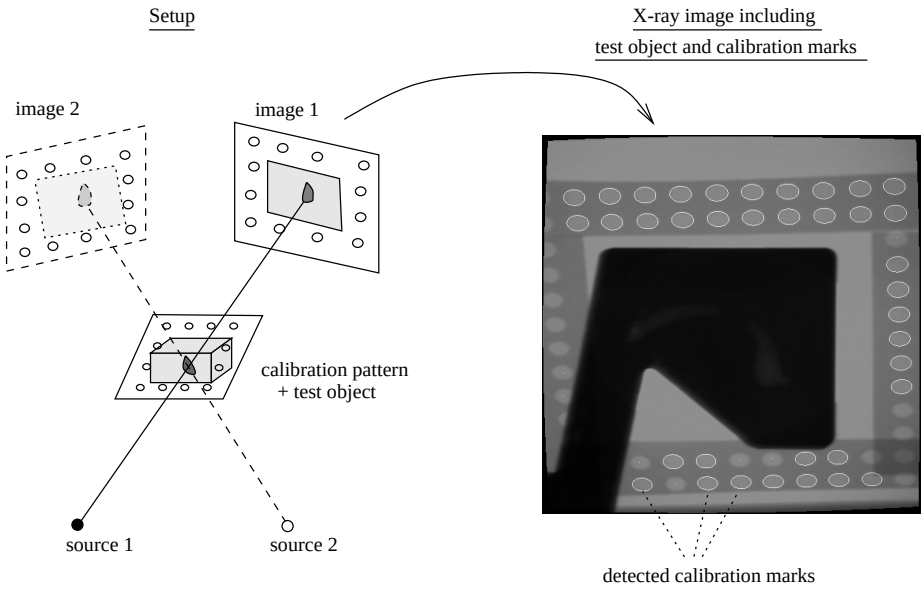

Fig. 3. Estimation of the parameters of the camera model

For the estimation of the spatial extent of the defect, called defect thickness $g_d(\boldsymbol{p_u})$, an estimate for the material thickness without the defect has to be estimated from the values of $g_b(\boldsymbol{p_u})$ outside the defect area. This is called a background model $g_h(\boldsymbol{p_u})$. Assuming locally smooth surfaces of the objects under investigation a two dimensional polynom of 3rd order according to Eq. 6 has been chosen for background interpolation.

$$g_h(x,y) = h_0 + h_1 \cdot x + h_2 \cdot y + h_3 \cdot x^2 + h_4 \cdot xy + ... + h_{14} \cdot x^2y^3 + h_{15} \cdot x^3y^3 \tag{6}$$

The segmentation starts by using some arbitrary automated defect detection method or a semiautomated interactive method incorporating a manual marking of regions of interest around the defect regions. This first estimate needs not to be accurate. From this first estimate the defect-free thickness $g_h(\boldsymbol{p_u})$ is estimated. The defect thickness $g_d(\boldsymbol{p_u})$ is calculated from the difference between $g_h(\boldsymbol{p_u})$ and $g_b(\boldsymbol{p_u})$. Using $g_d(\boldsymbol{p_u})$ the defect region can be localized more accurately. In further iterations the improved defect localization leads to an improved background estimation resulting in a further improvement of the defect segmentation. From the final result a good estimate of the defect extent in all three dimensions can be obtained.

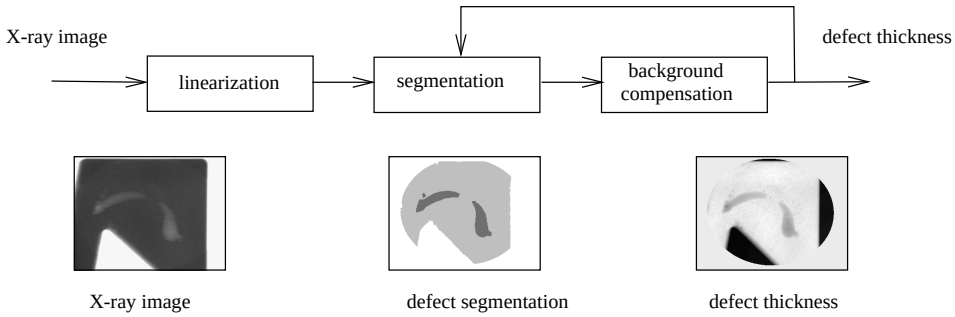

Fig. 4. Image segmentation: The X-ray image serves as input image. The defect segmentation constitutes a binary mask, indicating the precise location of the defect within the 2D image. The defect thickness represents a map indicating the estimated defect thickness for each point.

4 3D Reconstruction

The 3D reconstruction of the defect areas is carried out in an relaxation loop. The 3D volume which encloses the defect area is described by the discrete 3D voxel vector $\boldsymbol{\mu}$. $\boldsymbol{\mu}$ describes the material properties of the object under investigation. The values are normalized $0 \leq \mu(i) \leq 1$. Since the material is assumed to be homogeneous except for the defects, binary values are expected for $\mu(i)$: $\mu(d) = 1$ for the voxels belonging to the defect area and $\mu(o) = 0$ for the voxels belonging to the non-defect area. The relation between the measured and preprocessed data in the area of interest $\boldsymbol{p}$ and the binary material properties $\boldsymbol{\mu}$ are given by the matrix equation (7) where $\underline{A}$ describes the spatial relations, i.e. projection of the 3D volume space onto the different 2D radiographic views which have been recorded. The matrix value a_{ij} corresponds to the influence of the i-th voxel on the j-th projection.

$$\boldsymbol{p} = \underline{A} * \boldsymbol{\mu} \tag{7}$$

When only a few radiographs are used as had been proposed for the presented method, Eq. 7 turns out to be underdetermined. Inconsistent results may turn up due to errors in preprocessing, calibration errors, from both, the densiometric and the geometric calibration as well as due to different noise sources. The standard approach is to formulate additional constraints for the reconstruction process. These additional constraints are added to an energy function which has to be minimized and they have to be weighted by a regularization factor as is indicated in Eq. 8.

$$E = ||\underline{A} * \boldsymbol{\mu} - \boldsymbol{p}||^2 + \beta * E_R(\boldsymbol{\mu}) \tag{8}$$

As additional constraint the negative entropy $E_R(\boldsymbol{\mu})$ of the voxel vector has been chosen. Minimizing $E_R(\boldsymbol{\mu})$ is equivalent to maximizing the entropy. The minimization of the energy function E in Eq. 8 is achived using a modification of the MART algorithm for entropy maximization. Using the MART method the choice of the explicite regularizaton factor β in Eq. 8 is replaced by the choice of the relaxation parameter λ in Eq. 9.2. The modified MART algorithm, which has been used is the following:

1. Start with a strictly positive vector $\boldsymbol{\mu}^k$, $k = 0$
2. Calculate for all pixels j the actual projections $\tilde{p}_j^k$ and the new voxel values

$$\tilde{p}_j^k = \sum_i a_{ij} * \mu_i^k \tag{9.1}$$

$$\mu_i^{k+1} = \mu_i^k * \left(\frac{p_j}{\tilde{p}_j^k}\right)^{\lambda * a_{ij}} \tag{9.2}$$

3. Update all voxels according

$$\mu_i^{k+1} = \begin{cases} \mu_i^{k+1} \; if \; \mu_i^{k+1} \leq 1 \\ 1 \qquad if \; \mu_i^{k+1} > 1 \end{cases} \tag{9.3}$$

4. Update all voxel i every K.th iteration

$$\mu_i^{k+1} = median(\mu_i^{k+1}) \tag{9.4}$$

5. k=k+1
6. Repeat steps 2 to 6 until convergence

The first steps contain the basic MART algorithm. Depending on the noise properties of the data an adequate relaxation factor λ is selected automatically in order to guarantee a stable convergence of the procedure. Eq. 9.3 imposes the material constraints on the reconstruction. Finally, the repeated median filtering of the intermediate results leads to a clear improvement of the convergence behaviour. The noise properties of the measured data used for the choice of an adequate relaxation factor λ are estimated during the preprocessing procedure.

The minimization of the energy function E in Eq. 8 results in continuous material values $\boldsymbol{\mu}$ where low values indicate the tendency toward an non-defect property and high values the tendency towards a defect property. After the minimum of the E has been obtained using the modified MART algorithm thresholding is applied to $\boldsymbol{\mu}$ in order to update the defect area. Only the voxels with the largest material values are identified as belonging to the defect area. With the updated vector a new optimization cycle is started until the binary solution has been reached. In each iteration the threshold is automatically adapted to the current $\boldsymbol{\mu}$. The idea of this binarization procedure is to assign only a few voxels to the defect area in each iteration in order to ensure a gradual adjustment of the solution to the binary constraint.

5 Results

The performance of the suggested reconstruction method had at first been tested on simulated data. The complex test object of Fig. 5 has been chosen. It consists of a ball positioned within a convex hull. From this test object two sets of simulated X-ray views have been generated. Each set contains five different views within a range of 90°. The two sets differ in that one set has been augmented with noise in order to test the robustness of the reconstruction method. The surface of the simulated object, one sample of a simulated view from each set and the surface of the reconstructed 3D object are shown in Fig. 5. As can be seen the reconstructions almost match the shape of the original object except for some slight differences at the lower part of the convex hull in case of the noise deteriorated data.

Real data have been processed with known and unknown geometric properties. In both cases the X-ray images have first been rectified for geometrical distortions and the camera parameters have been estimated. Geometric distortions of sometimes more than 11 pixels could be reduced to less than 0.3 pixel.

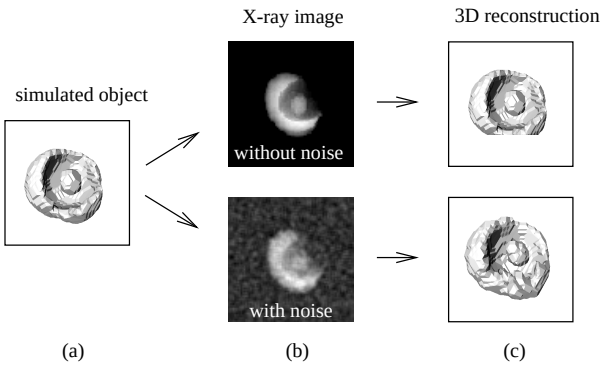

Fig. 5. Reconstruction of a simulated object: (a) shape of the test object, (b) simulated X-ray views with and without added noise, (c) shape of reconstructed object

A test object with known geometric properties consists of a plate with drilling holes of different depth and diameter. Five views have been acquired within a range of 60°. All reconstruction errors appear in the border region on the surface. The deviation from the real shape is in the average less than one voxel. The maximum deviation amounted to 2 voxels. The test object and its 3D reconstruction are depicted in Fig. 6 on the left side.

Fig. 6 (left side) shows the reconstruction of casting defects with geometric properties which have not be known before. This and the other tests demon-

strate very well that it is possible to reconstruct the 3D shape of objects from a few X-ray images taken from different views with standard X-ray systems and without special positioning equipment.

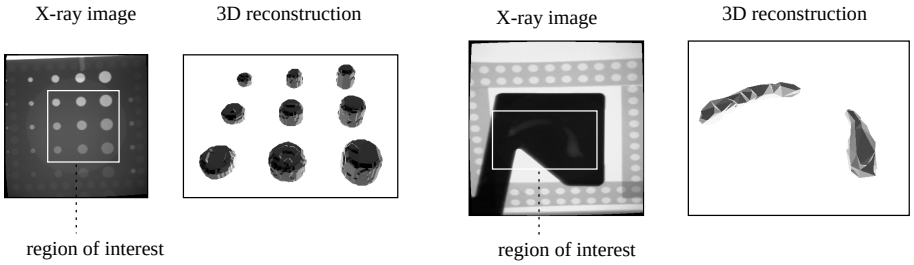

Fig. 6. Reconstruction of drilling holes and casting defects

References

1. Herman,G.T.: Image Reconstruction from Projections. The fundamentals of Computerized Tomography. Academic Press, 1980.
2. Kak, A. C.; Slaney, M.: Principles of Computerized Tomographic Imaging. New York, IEEE Press, 1988.
3. Robert, N.; Peyrin, F.; Yaffe, M.J.: Blodd vessel reconstruction from a limited number of cone-beam projections: Application to cerebral blood vessel projections and to an excise animal heart. Annual SPIE Conference on Machine Vision Applications in Industrial Inspection, San Jose, Cal., 1995, SPIE proc. series 2423.
4. Stegemann, D.: Zerströungsfreie Prüfverfahren: Radiographie und Radioskopie. B.G. Teubner, Stutgart, 1995.
5. Djafari, A.M.: Shape Reconstruction in X-Ray Tomography. Image Reconstruction and Restoration 2, San Diego, California, 1997, SPIE Vol. 3170.
6. Milanfar, P.; Karl, W.C.; Willesky, A.S.: Reconstructing Binary Polygonal Objects from Projections: A Statistical View. Graphical Models and Image Processing, Vol 56, 5, 1994.
7. Retraint, F.; Peyrin, F.; Dinten, J.M.: Three-Dimensional Regularized Binary Image Reconstruction From Two-Dimensional Projections Using a Randomized ICM Algorithmus. Int. J. of Imag. Systems Technology, pp. 135-146, Vol 9, 1998.
8. Yakimovski, Y.; Cunningham, R.: A System for Extraction Three-Dimensional Measurement from a Stereo Pair of TV Cameras. Intern. Journal on Computer Graphics and Image Processing.Vol 7, S. 195-210, 1978.
9. Lehr, C.; Feiste, K.; Stegeman, D.; Liedtke, C.-E.: Three dimensional defect analysis using stereoradioscopy based on camera modelling. 7.ECNDT Conference, Copenhagen, 1998.
10. Tsai, R.Y.: A versatile camera calibration technique for high-accuracy 3D machine vision meterology using off-the-shell tv cameras and lenses. IEEE J.Robotics Automation, Vol. RA-3(4), August 1988, S. 323-344.